GMR
The Original

# DEVELOPMENT AND CHARACTERIZATION OF LAPPAOL F LOADED FUNCTIONALIZED SOLID LIPID NANOCARRIERS FOR TARGETED DELIVERY IN CANCERS

**Jyotiraditya Fiske[1], Dr. Amol S. Rakte[1*], Dr. Payal K Thorat[2], Dr. Sanjay R. Arote[3]**

[1,2]Department of Pharmaceutics, Indrayani Vidya Mandir's Krishnarao Bhegade Institute of Pharmaceutical Education and Research, Talegaon Dabhade, Tal-Maval, Pune-410507, Maharashtra, India
[3]Department of Pharmacology, Indrayani Vidya Mandir's Krishnarao Bhegade Institute of Pharmaceutical Education and Research, Talegaon Dabhade, Tal-Maval, Pune-410507, Maharashtra, India

**Abstract**

**Objectives:** To develop, optimize, and characterize lactoferrin-functionalized Lappaol F-loaded solid lipid nanocarriers (Lf-LpF-SLNs) for targeted anticancer delivery, addressing the poor solubility and limited bioavailability of Lappaol F.

**Methods:** Lappaol F-loaded solid lipid nanocarriers were prepared by melt emulsification–probe sonication and optimized using a three-factor, three-level Box–Behnken Design (BBD) with Compritol 888 ATO concentration, Poloxamer 188 concentration, and probe sonication pulse duty cycle as independent variables. The optimized formulation was surface functionalized with lactoferrin via EDC/NHS coupling, followed by evaluation of physicochemical properties, drug release, stability, and in vitro cytotoxicity.

**Results:** The quadratic models for particle size ($R^2 = 0.8109$) and entrapment efficiency ($R^2 = 0.8370$) were statistically significant ($p < 0.05$). Optimized batch JF10 (desirability 0.924) showed particle size of 1726 ± 4.34 nm, PDI 0.178 ± 0.016, zeta potential −30.4 ± 1.22 mV, and entrapment efficiency 81.46 ± 1.68%. Lactoferrin conjugation was confirmed by FTIR through Amide I (1653 $cm^{-1}$) and Amide II (1545 $cm^{-1}$) bands. Lf-LpF-SLNs exhibited enhanced cytotoxicity ($IC_{50}$ 14.82 ± 0.92 µg/mL) compared to LpF-SLNs (21.38 ± 1.06 µg/mL) and free Lappaol F (28.64 ± 1.24 µg/mL). Stability was confirmed over six months under accelerated conditions.

**Conclusion:** Lf-LpF-SLNs represent a promising receptor-targeted nanocarrier system with improved tumor selectivity and cytotoxic efficacy, warranting further in vivo investigation.

**KEYWORDS:** Lappaol F; Solid lipid nanocarriers; Lactoferrin functionalization; Box-Behnken Design; Targeted drug delivery; Breast cancer.

**GRAPHICAL ABSTRACT**


## INTRODUCTION

Cancer continues to be one of the most difficult public health challenges facing humanity in the 21st century, accounting for about 19.3 million new cases and causing nearly 10 million deaths worldwide in 2020 with rising trajectories towards 28.4 million cases by 2040 [1]. Breast, colorectal, lung and hepatocellular carcinomas contribute to the majority of the highest disease burden in an increasingly globalized world where diverse cancer types disproportionately affect low- and middle-income countries with severely limited access to modern therapeutic armamentarium [2]. In addition, with ageing populations and rising incidence rates, the economic burden of cancer worldwide surpassed USD 1.16 trillion in 2010 and

treatment costs continue to climb [3]. Current standard-of-care approaches, like surgery, radiation and traditional chemotherapy are restricted by systemic toxicity, drug resistance, poor tumor selectivity and suboptimal pharmacokinetic profiles. Despite great progress in targeted therapy and immunotherapy, a substantial number of patients do not experience durable responses [4]. Indeed, the absence of tumor-specific delivery systems capable of addressing biological hurdles including but not limited to enhanced permeability and retention (EPR) effect, multidrug resistance (MDR), and off-target toxicity reaffirms the critical demand for novel therapeutic platforms that can facilitate superior therapeutic outcomes with minimal adverse effects [5].

Lappaol F, a dibenzylbutyrolactone-type lignan obtained from Arctium lappa L. (burdock), represents a promising anticancer phytochemical molecule with clinical applications. Lappaol F, a bicyclic lactone with two phenylpropanoid side chains substituted with hydroxyl and methoxy groups, engages favorably multiple oncogenic targets [6]. Its antitumor activity is mediated by mechanisms including G1/S phase arrest, initiation of intrinsic pathways of apoptosis through reduced mitochondrial membrane potential and a relative increase in pro-apoptotic Bax to anti-apoptotic Bcl-2 protein ratio [7]. In vitro and in vivo results demonstrating considerable cytotoxic activity against MCF-7 breast cancer, HepG2 hepatocellular carcinoma, and A549 non-small cell lung cancer cell lines have been reported recently. In addition, the effects of Lappaol F on the inhibition of tumor angiogenesis and suppression of EMT are closely associated with cancer metastasis [8]. Despite broad therapeutic potential, Lappaol F is BCS Class IV (poor aqueous solubility) and has drawbacks of rapid hepatic metabolism, poor oral bioavailability, and short plasma half-life, thus an advanced drug delivery strategy is required to maximize its clinical utility [9].

Solid lipid nanocarriers (SLNs) have received a great deal of scientific attention as a broad-spectrum drug delivery system for hydrophobic bioactive components, due to their physical and chemical characteristics such as lipophilicity, high scalability and biocompatibility [10]. Solid lipid nanoparticles (SLNs) consist of physiologically tolerable solid lipids that are stabilized by biocompatible surfactants, leading to a protective lipid matrix that facilitates solubilization of drug molecules, regulates release kinetics, and prolongs blood circulation [11]. In addition, the active targeting ligands such as folic acid, transferrin, hyaluronic acid and monoclonal antibodies can be functionalized to combine with specific receptors on tumor cells which could mediate receptor-mediated endocytosis to increase drug deposit at targeted sites while decreasing off-target toxicity [11]. Compared with conventional lipid emulsions and polymeric nanoparticles, novel SLNs have shown better capacity for cellular uptake, endosomal escape, and intracellular drug release [12]. Further, functionalized SLNs exploit the enhanced permeability and retention (EPR) effect in solid tumors promoting passive targeting as a synergy to active ligand-receptor interaction. These systems have shown significant advantage in co-delivering chemosensitizers with phytochemicals, surmounting multidrug transporters. In summary, the rational design of Lappaol F-loaded functionalized SLNs proposed in this work is a scientifically sound and clinically translatable strategy to overcome the existing delivery hurdles associated with this promising bioactive lignan [13].

To design, optimize and characterize Lappaol F-loaded functionalized solid lipid nanocarriers targeting anticancer delivery is the objective of current research. The specific aims include: optimization of formulation variables by implementation of quality-by-design (QbD) principles, physicochemical characterization, in vitro drug release profiling, cytotoxicity testing on chosen cancer cell types, and cellular uptake and targeting efficacy to validate preclinical proof-of-concept for this nanocarrier platform.

## MATERIALS AND METHODS

### MATRIALS

Lappaol F (analytical grade, purity ≥98%) was obtained from Sciquaint Innovations Pvt. Ltd., Pune, India. Compritol 888 ATO (Pharmaceutical grade), Poloxamer 188 (Pharmaceutical grade), Soya lecithin (Pharmaceutical grade), Tween 80 (Pharmaceutical grade) and Stearic acid were procured from Sciquaint Chemicals, Pune, India. Lactoferrin (biochemical grade, bovine origin, purity ≥ 90%), EDC·HCl and NHS (both analytical grade) were procured from Neeta Chemicals, Pune, India. Methanol and acetonitrile (HPLC grade), DMSO, ethanol, and potassium bromide (IR grade) were purchased from Research Lab Fine Chem Industries, Mumbai, India. DMEM, FBS and MTT reagent (all cell culture grade) were purchased from Sciquaint Chemicals, Pune, India. All other chemicals and reagents were of analytical grade and without further purification and used as received.

### METHODS

#### Calibration Curve Determination of Lappaol F

A calibration curve of Lappaol F in methanol was established by preparing a primary stock solution (1000 µg/mL) and subsequent working standard solutions at the following concentrations: 5, 10, 15, 20, 25 and 30 µg/mL using appropriate serial dilution in HPLC-grade methanol (Merck Life Sciences Pvt. Ltd., Mumbai, India). The absorbance of individual solutions (n = 3) was recorded against methanol as blank at previously chosen λmax using a double-beam UV-Visible spectrophotometer (Systronics UV-2203, Systronics India Ltd., Ahmedabad, India), fitted with quartz cuvettes of 1 cm path length. A concentration (µg/mL) vs mean absorbance calibration graph was plotted and linear regression analysis used to obtain the regression equation ($y = mx + c$), slope, intercept, and coefficient of determination ($r^2$) as per ICH Q2(R1). All data are presented as mean ± SD [14].

#### Solubility Study of Lappaol F

The solubility of Lappaol F was determined prior to its test in both physiologically relevant and organic solvents such as distilled water, phosphate buffer pH 6.8, phosphate buffer pH 7.4, simulated body fluid (SBF), methanol, ethanol, DMSO and acetonitrile. A large amount of Lappaol F (approximately 50 mg) was poured into each solvent, in separate stoppered

conical flasks, prepared for continuous shaking at 100 rpm for 24 h at 37 ± 0.5 °C using an orbital shaker (Remi Instruments Ltd., Mumbai, India). The suspensions were allowed to stand for 30 min, filtered via Whatman No. 41 filter paper (Whatman, Kent, UK), suitably diluted and absorbance was measured at predetermined λmax by double-beam UV-Visible spectrophotometer (Systronics UV-2203; Systronics India Ltd., Ahmedabad, India). Values of solubility were determined from the equation of the calibration curve and expressed as mg/mL (n = 3, mean ± SD) [15].

**Differential Scanning Calorimetry (DSC)**

A differential scanning calorimeter (Mettler Toledo DSC 822e, Mettler Toledo India Pvt. Ltd., Mumbai, India) was used. For differential scanning calorimetry (DSC), accurately weighed portions (~3–5 mg) of pure Lappaol F and its physical mixture with the prepared excipients were crimped into hermetically sealed aluminum pans and an empty sealed pan was used as reference. The samples were heated at a scanning rate (10°C/min) over 30–300°C in an inert nitrogen atmosphere (purge flow: 20 mL/min) to avoid oxidative decomposition. The resultant thermograms were examined for characteristic endothermic or exothermic transitions, determining onset temperature, peak temperature, and enthalpy changes (ΔH), which upon peak shifts/disappearances were interpreted as an indication of drug-excipient incompatibility or crystalline state alteration. Each measurement was done in triplicate (n = 3) and results were expressed as mean ± SD [16].

**Fourier Transform Infrared Spectroscopy (FTIR)**

A Fourier transform infrared spectrophotometer (Shimadzu IRTracer-100, Shimadzu Analytical India Pvt. Ltd., Mumbai, India) using the KBr pellet method. Approximately 2–3 mg of pure Lappaol F and its physical mixture with excipients were separately ground in a clean mortar and pestle for 5–10 min to ensure homogeneous mixing with pre-dried KBr powder (~200 mg, dried for 2 h at 40–50°C). The mixture was then pressed for 3–5 min under hydraulic pressure (~10 tons) into a transparent, self-supporting disc with the use of a hydraulic press and immediately inserted in the sample holder for spectral acquisition. Spectra were obtained in KBr pellets from wavenumbers of 4000–400 $cm^{-1}$, at a resolution of 4 $cm^{-1}$ with 32 scans per sample (reference = blank KBr pellet). The recorded spectra were examined for prominent absorption bands related to functional groups of Lappaol F and the occurrence of significant peak shifts, broadening, or disappearances in the physical mixture spectra was taken as indicative of possible drug-excipient interaction. All analyses were done in triplicate (n = 3) [17].

**Preliminary Trial Batches for Excipient Concentration Selection**

In a preliminary approach, different batches of Lappaol F-loaded solid lipid nanocarriers (TB1–TB6) were formulated by means of the melt emulsification–probe sonication method to find appropriate concentration ranges for three key formulation variables: Compritol 888 ATO (% w/v), Poloxamer 188 (% w/v) and probe sonication pulse duty cycle (% pulse-ON). Drug content was constant at 0.5% w/v and soya lecithin at 0.75% w/v for all the batches. Particle size (nm), polydispersity index (PDI), zeta potential (mV), and entrapment efficiency (%EE) of each batch were determined. Acceptance criteria were determined as particle size < 250 nm, PDI < 0.3, zeta potential ≤ −20 mV and %EE > 60%. All measurements were performed in triplicate (n = 3) and presented as mean ± SD [18].

**Table 1: Composition and Results of Preliminary Trial Batches**

| Batch | Compritol 888 ATO (% w/v) | Poloxamer 188 (% w/v) | Pulse Duty Cycle (%) | Particle Size (nm) | PDI | Zeta Potential (mV) | %EE |
|---|---|---|---|---|---|---|---|
| TB1 | 2.0 | 0.5 | 60 | 418 ± 19.2 | 0.54 | −13.8 ± 1.4 | 46.2 ± 2.3 |
| TB2 | 3.0 | 0.5 | 60 | 302 ± 13.8 | 0.39 | −17.4 ± 1.2 | 55.6 ± 1.9 |
| TB3 | 3.0 | 1.0 | 60 | 214 ± 8.6 | 0.23 | −24.1 ± 1.3 | 67.4 ± 2.1 |
| TB4 | 4.0 | 1.0 | 60 | 188 ± 7.4 | 0.19 | −27.6 ± 1.5 | 73.8 ± 2.4 |
| TB5 | 5.0 | 1.5 | 60 | 176 ± 6.9 | 0.17 | −29.8 ± 1.6 | 77.5 ± 1.8 |
| TB6 | 6.0 | 2.0 | 60 | 316 ± 15.4 | 0.43 | −15.2 ± 1.1 | 63.4 ± 2.7 |

Based on these results, the concentration ranges selected for experimental design were: Compritol 888 ATO (3–5% w/v), Poloxamer 188 (0.5–1.5% w/v), and probe sonication pulse duty cycle (40–80% pulse-ON).

**Experimental Design for Formulation Optimization**

For method optimization, a three-factor and three-level Box-Behnken Design (BBD) was employed using Design Expert® software (Version 13.0, Stat-Ease Inc., USA), to improve the formulation of Lappaol F-loaded solid lipid nanocarrier (LpF-SLN). Independent variables were chosen as concentration of Compritol 888 ATO ($X_1$, % w/v), concentration of Poloxamer 188 ($X_2$, % w/v) and probe sonication pulse duty cycle (X3, % pulse-ON time). As a new independent variable never explored as part of any functionalized lignan-loaded solid lipid nanocarrier, the pulse duty cycle defined as the ratio of sonication ON-time to total cycle time expressed as percentage was introduced. Although previous literature has varied sonication amplitude or duration, the pulse duty cycle can modulate cumulative energy delivery per unit time independently and consequently exerts a distinct and unexplored influence on nanoparticle formation dynamics. Two responses (dependent variables) were chosen: particle size $Y_1$ (nm)—minimization—and percentage entrapment efficiency Y2 (%EE) — maximization. In total, 17 experimental runs were generated including five center-point replicates. Each response is related to the independent variables using a quadratic polynomial model:

$$Y = \beta_0 + \beta_1X_1 + \beta_2X_2 + \beta_3X_3 + \beta_{12}X_1X_2 + \beta_{13}X_1X_3 + \beta_{23}X_2X_3 + \beta_{11}X_1^2 + \beta_{22}X_2^2 + \beta_{33}X_3^2$$

Where Y is the measured response; $\beta_0$ is intercept; $\beta_1$, $\beta_2$, $\beta_3$ are linear coefficients; $\beta_{12}$, $\beta_{13}$, $\beta_{23}$ coefficients of interactions; and $\beta_{11}$,β22, β33 are quadratic coefficients for Compritol 888 ATO concentration, Poloxamer 188 concentration and probe

sonication pulse duty cycle respectively. Model validation was carried out through ANOVA ($p < 0.05$), and the most suitable formulation was determined by a numerical desirability function [19,20].

**Table 2: Box-Behnken Design Independent and Dependent Variables**

| | Variable | −1 (Low) | +1 (High) |
|---|---|---|---|
| **Independent Variables** | $X_1$: Compritol 888 ATO (% w/v) | 3.0 | 5.0 |
| | $X_2$: Poloxamer 188 (% w/v) | 0.5 | 1.5 |
| | $X_3$: Probe sonication pulse duty cycle (% pulse-ON) | 40 | 80 |
| **Dependent Variables** | $Y_1$: Particle size (nm) | | Goal: Minimize |
| | $Y_2$: Entrapment efficiency (% EE) | | Goal: Maximize |

**Table 3: Composition of all batches as per Box-Behnken Design**

| Formulation | Lappaol F (% w/v) | Compritol 888 ATO (% w/v) | Soya Lecithin (% w/v) | Poloxamer 188 (% w/v) | Tween 80 (% w/v) | Pulse Duty Cycle (% ON) |
|---|---|---|---|---|---|---|
| F1 | 0.5 | 3.0 | 0.75 | 0.5 | 0.1 | 60 |
| F2 | 0.5 | 5.0 | 0.75 | 0.5 | 0.1 | 60 |
| F3 | 0.5 | 3.0 | 0.75 | 1.5 | 0.1 | 60 |
| F4 | 0.5 | 5.0 | 0.75 | 1.5 | 0.1 | 60 |
| F5 | 0.5 | 4.0 | 0.75 | 0.5 | 0.1 | 40 |
| F6 | 0.5 | 4.0 | 0.75 | 1.5 | 0.1 | 40 |
| F7 | 0.5 | 4.0 | 0.75 | 0.5 | 0.1 | 80 |
| F8 | 0.5 | 4.0 | 0.75 | 1.5 | 0.1 | 80 |
| F9 | 0.5 | 3.0 | 0.75 | 1.0 | 0.1 | 40 |
| F10 | 0.5 | 5.0 | 0.75 | 1.0 | 0.1 | 40 |
| F11 | 0.5 | 3.0 | 0.75 | 1.0 | 0.1 | 80 |
| F12 | 0.5 | 5.0 | 0.75 | 1.0 | 0.1 | 80 |
| F13–F17 | 0.5 | 4.0 | 0.75 | 1.0 | 0.1 | 60 |

Soy lecithin (0.75% w/v) and Tween 80 (0.1% w/v) were kept constant. Total volume adjusted to 25 mL with ultrapure water. F13–F17 are center-point replicates.

**Preparation of Lappaol F-Loaded Solid Lipid Nanocarriers (LpF-SLNs)**

LpF-SLNs were prepared by the melt emulsification and pulsed probe sonication method. The lipid phase was prepared by melting Compritol 888 ATO (as such), soya lecithin (0.75% w/v) and Lappaol F (0.5% w/v) on a hot-plate magnetic stirrer (Remi Equipment, Mumbai, India) at 80 ± 2°C. A hot aqueous phase consisting of Poloxamer 188 (as such), and Tween 80 (0.1% w/v) in ultrapure water (25 mL), was prepared separately by heating at 80 ± 2 °C, then added dropwise into the molten lipid phase during high-speed homogenization at 10,000 rpm for a duration of 5 min with the aid of a high-speed homogenizer [IKA T25 digital Ultra-Turrax, IKA, Germany], producing a primary hot nanoemulsion. The nanoemulsion was probe-sonicated (Sonics Vibracell VC-505, Sonics & Materials Inc., USA) for 5 min at an amplitude of 40% with the duty cycle adjusted according to the experiment design (40%, 60%, or 80% pulse-ON). Hot sonicated dispersion was immediately dispersed in cold ultrapure water (2–4 °C) under magnetic stirring at 500 rpm for solidifying lipid droplets. The resulting dispersion was then cooled at 25 °C and preserved at 4 °C [21,22].

**Lactoferrin Functionalization of Optimized LpF-SLNs (Lf-LpF-SLNs)**

Among them, Lactoferrin (Lf) was chosen as the single targeting ligand for surface functionalization of the optimized LpF-SLNs. Lactoferrin binds simultaneously to LRP1/2 (low-density lipoprotein receptor-related proteins) and lactoferrin-specific receptors that are overexpressed in various solid tumors, rendering it an intrinsically bifunctional targeting vehicle. The present study is the first literature report on such lactoferrin-functionalized Lappaol F loaded SLNs (Lf-LpF-SLNs) thereby clearly enhancing novelty in the field of functionalization towards in vivo delivery of lignan class anticancer drugs. We performed conjugation via a carbodiimide-mediated strategy of covalent coupling. For macromolecular conjugation, lactoferrin (Sigma-Aldrich, Bangalore, India) (5 mg), dissolved in PBS (pH 6.0, 2 mL), was added to the solid nanoparticle-forming solution containing activated carboxyl groups on the nanoparticle surface (the incorporated stearic acid during preparation of lipid phase produces surface –COOH groups) after activation with EDC·HCl (10 mg) and NHS (6 mg) in PBS buffer at pH 6.0 for 30 minutes at room temperature under gentle stirring. The activated nanoparticle dispersion was then mixed with the lactoferrin solution at a ratio of 0.5 mg lactoferrin per mg nanoparticle and coupling reaction was carried out over a period of 12 hours at 4°C while stirring gently in dark. Dialysis against PBS (pH 7.4, 24 h, in a dialysis membrane of MWCO 12–14 kDa; HiMedia Laboratories, Mumbai, India) by changing buffer every 6 h was performed to remove unreacted lactoferrin and coupling reagents at 4°C. Purified Lf-LpF-SLNs were lyophilized by using a lyophilizer (Christ Alpha 1-2 LD plus, Christ, Germany) in the presence of mannitol (5% w/v), and stored at −20°C until used in the studies after reconstituting them with ultrapure water [23].

**Characterization of LpF-SLNs and Lf-LpF-SLNs**

**Particle Size, Polydispersity Index (PDI), and Zeta Potential**

The particle size, PDI and zeta potential of all formulations including LpF-SLNs and Lf-LpF-SLNs were evaluated by dynamic light scattering (DLS) and laser Doppler electrophoresis, respectively, with the Zetasizer Nano ZS90 (Malvern Instruments, UK). Samples were diluted 1:100 (v/v) with ultrapure water before measurement to minimize multiple scattering effects and measured at a temperature of 25 °C at a backscatter detection angle of 173°. Particle size was reported as the Z-average hydrodynamic diameter (nm) and PDI, indicative of the uniformity in particle size distribution; values less than 0.3 were considered reflective of a monodisperse, pharmaceutically acceptable system Electrostatic stability (zeta potential) was determined in disposable folded capillary cells (DTS1070) using phase analysis light scattering (PALS), with any value more negative than −20 mV deemed appropriate for electrostatic stabilization. Since binding of a protein layer changes surface charge, a shift in zeta potential relative to unconjugated LpF-SLNs served as an early marker for successful conjugation of lactoferrin onto their surfaces for Lf-LpF-SLNs. All measurements were conducted three times (n = 3) and presented as mean ± SD [24,25].

**Entrapment Efficiency (%EE) and Drug Loading (%DL)**

The entrapment efficiency percentage and drug loading of LpF-SLNs and Lf-LpF-SLNs were determined by the indirect ultracentrifugation method. Following preparation, 1 mL of the nanoparticle dispersion was subjected to ultracentrifugation at 15,000 rpm for 30 minutes at 4°C. The supernatant containing unentrapped free Lappaol F was collected and spectrophotometrically quantitated at wavelength λ = 263 nm (UV-1800; Shimadzu, Kyoto, Japan) after appropriate dilution with methanol using a previously validated calibration curve ($y = 0.0367x + 0.0022$, $r^2 = 0.9999$). Equations used to determine %EE and %DL were as follows:

$$\text{Entrapment Efficiency (\%)} = \left[\frac{\left(\text{Total drug added-Free drug in supernatant}\right)}{\text{Total drug added}}\right]\times 100$$

$$\text{\% Drug Loading} = \left[\frac{\left(\text{Total drug added-Free drug in supernatant}\right)}{\text{Total weight of nanoparticle recovered}}\right]\times 100$$

The total weight of nanoparticles recovered was determined gravimetrically after lyophilization of a known volume of dispersion. All determinations were performed in triplicate (n = 3) and expressed as mean ± SD [26,27].

**Morphological Characterization by Transmission Electron Microscopy (TEM)**

The morphology and particle size of LpF-SLNs and Lf-LpF-SLNs were determined by transmission electron microscope (JEOL JEM-2100, JEOL Ltd., Japan). A small amount of appropriately diluted nanoparticle dispersion (1:100 v/v in ultrapure water) was deposited on a carbon formvar-coated 300-mesh copper grid and adsorbed for 2 min. The excess sample was blotted with filter paper and the grid negatively stained first with one drop of 2% (w/v) aqueous phosphotungstic acid for 2 minutes at 25°C, subsequently air dried and examined at an accelerating voltage of 80 kV at magnifications of 50,000–100,000×. Representative micrographs were obtained to verify spherical morphology, nanoscale size and uniformity. A well-defined peripheral electron-dense protein layer (compared to unconjugated LpF-SLNs) on the Lf-LpF-SLNs surface was considered as indicative of successful lactoferrin decoration [28,29].

**In Vitro Drug Release**

In vitro Lappaol F release study of LpF-SLNs and Lf-LpF-SLNs was carried out using dialysis bag diffusion approach at physiological conditions. Dialysis bags (MWCO 12–14 kDa; HiMedia Laboratories, Mumbai, India) were hydrated with PBS (pH 7.4) for 12 hours before preparation. The nanoparticle dispersion equivalent to 1 mg of Lappaol F was placed in the dialysis bag, which was inserted into 200 mL PBS (pH 7.4) kept at 37 ± 0.5°C and stirred using a magnetic stirrer ($R^2$emi Equipment, Mumbai, India) at a speed of 100 rpm for continuous agitation. Aliquots (2 mL) were withdrawn at predetermined intervals of time (0.5, 1, 2, 4, 6, 8, 12, 24 and up to 48 h) and replaced with equal volumes of fresh PBS in order to maintain sink conditions. The concentration of Lappaol F in each withdrawn aliquot was spectrophotometrically measured at 263 nm (UV-1800, Shimadzu, Kyoto, Japan) after proper dilution with methanol. Cumulative percentage drug release was derived from a validated calibration curve equation. A free drug suspension (1 mg/mL Lappaol F in PBS containing 0.5% w/v Tween 80) treated similarly was used as the comparative control. The release kinetics were assessed by fitting the cumulative release data to zero-order, first-order, Higuchi matrix and Korsmeyer-Peppas equations using the DDSolver software; The model with the maximum coefficient of determination (R) and minimal Akaike information criterion (AIC) was considered as best fit model. All the experiments were done in triplicate (n = 3) and data are represented as mean ± SD [30,31].

**Stability Studies**

The physical and chemical stability behavior of optimized Lf-LpF-SLNs was determined as per the ICH Q1A(R2) guidelines. The lyophilized samples were reconstituted and stored at long-term (25 ± 2 °C/60 ± 5% RH) and accelerated conditions (40 ± 2 °C/75 ± 5% RH) in a stability chamber (Thermolab Scientific Equipments, Mumbai, India) for up to the period of 3 months. At 0, 1, 2 and 3 months samples were withdrawn and assessed for particle size, PDI, zeta potential and %EE. Any substantial alteration in these parameters when compared to the initial values was regarded as evidence of the physical or chemical instability. Statistical analysis was performed by one-way ANOVA followed by Tukey's post hoc test, using GraphPad Prism 9.0 (GraphPad Software, USA), with $p < 0.05$ as significance level. All measurements were done in triplicate (n = 3) and represented as mean ± SD [32,33].

**In Vitro Cytotoxicity (MTT Assay)**

The MTT-assay was performed to evaluate the cytotoxicity of free Lappaol F, LpF-SLNs and Lf-LpF-SLNs against the human breast adenocarcinoma (MCF-7) cell line. Cells were seeded at $5 \times 10^3$ cells/well in DMEM containing 10% FBS and maintained at 37°C in a humidified $CO_2$ incubator (5% $CO_2$; Thermo Scientific, USA) on 96-well flat-bottom plates for 24 hours. The six concentrations of each test formulation (1, 5, 10, 25, 50 and 100 µg/mL based on Yappenol equivalent) were added and incubated for a period of 48 hours. MTT reagent (5 mg/mL in PBS, 20 µL/well) was subsequently added and incubated for 4 hours at 37°C; formazan crystals were dissolved in 100 µL DMSO per well, and absorbance was measured at 570 nm (reference wavelength:630 nm) using an ELISA plate reader (BioTek Instruments, USA). Percentage values of cell viability were calculated with respect to untreated control wells and $IC_{50}$ values determined by non-linear regression in GraphPad Prism 9.0 (GraphPad Software, USA). All experiments were done in triplicate (n = 3) and expressed as the mean ± SD [34–36].

## RESULTS AND DISCUSSION

## RESULTS

### Calibration Curve of Lappaol F

As shown in Figure 1, the calibration curve of Lappaol F in methanol revealed a good linearity within the studied concentration range (5–30 µg/mL). The regression equation y = 0.0367x + 0.0022 was computed (with a correlation coefficient ($R^2$) of 0.9999), confirming that Beer-Lambert law compliance was strict in the studied concentration range. As depicted in Table 1, the high value of R2 ensured the reliability and reproducibility of the method, which could therefore be safely applied for accurate quantification of Lappaol F during all subsequent studies involving formulations.

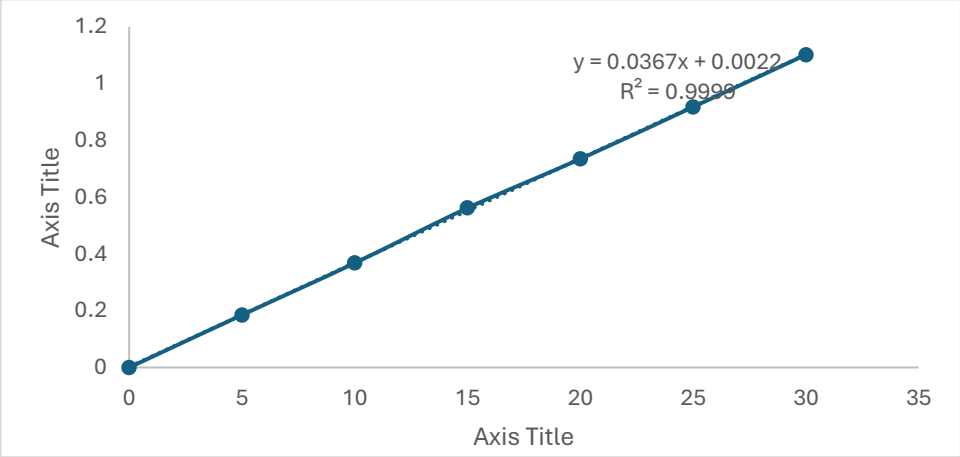


**Figure 1: Calibration curve of Lappaol F in methanol**

### Results of Solubility Study

The solubility behavior of Lappaol F in a variety of physiologically pertinent and organic solvents is presented in Table 4. The soluble concentrations of Lappaol F were 0.08 ±0.012, 0.12 ±0.018, 0.14 ±0.021 and 0.09 ± 0.015 mg/mL when it was dissolved in distilled water, phosphate buffer pH7.4, phosphate buffer pH6.8 and simulated body fluid respectively [17]. The drug, on the other hand, exhibited high solubility in organic solvents with it being found to be freely soluble in DMSO (125.6 ± 5.42 mg/mL) and soluble in methanol (45.8 ± 2.34 mg/mL), acetonitrile (42.5 ± 2.18 mg/mL) and ethanol (38.2 ± 1.87 mg/mL), supporting that Lappaol F has highly lipophilic nature which makes the development of lipid-based nanocarrier systems justifiable.[12

**Table 4: Solubility Profile of Lappaol F in Different Solvents**

| Sr. No. | Solvent | Solubility (mg/mL) | Inference |
|---|---|---|---|
| 1 | Distilled Water | 0.08 ± 0.012 | Practically insoluble |
| 2 | Phosphate Buffer pH 7.4 | 0.12 ± 0.018 | Practically insoluble |
| 3 | Phosphate Buffer pH 6.8 | 0.14 ± 0.021 | Very slightly soluble |
| 4 | Simulated Body Fluid (SBF) | 0.09 ± 0.015 | Practically insoluble |
| 5 | Methanol | 45.8 ± 2.34 | Soluble |
| 6 | Ethanol | 38.2 ± 1.87 | Soluble |
| 7 | Dimethyl Sulfoxide (DMSO) | 125.6 ± 5.42 | Freely soluble |
| 8 | Acetonitrile | 42.5 ± 2.18 | Soluble |

### DSC Analysis

Figure 2 shows the DSC thermograms of pure Lappaol F and its physical mixture with formulation excipients. Pure Lappaol F showed a typical endothermic peak at 148.05°C (Figure 2A), which confirmed its crystallinity and corresponds excellently to the observed melting point from the range of 148–152°C determined here. The thermogram of pure physical mixture (Figure 2B) kept the drug melting endotherm at 148.91°C with slight displacement, in addition to a second peak

at 187.44°C related to thermal transitions of excipients. Confirmation of non-chemical interactions between Lappaol F and formulation excipients was established by the absence of new peaks or significant shifting of the drug endotherm.

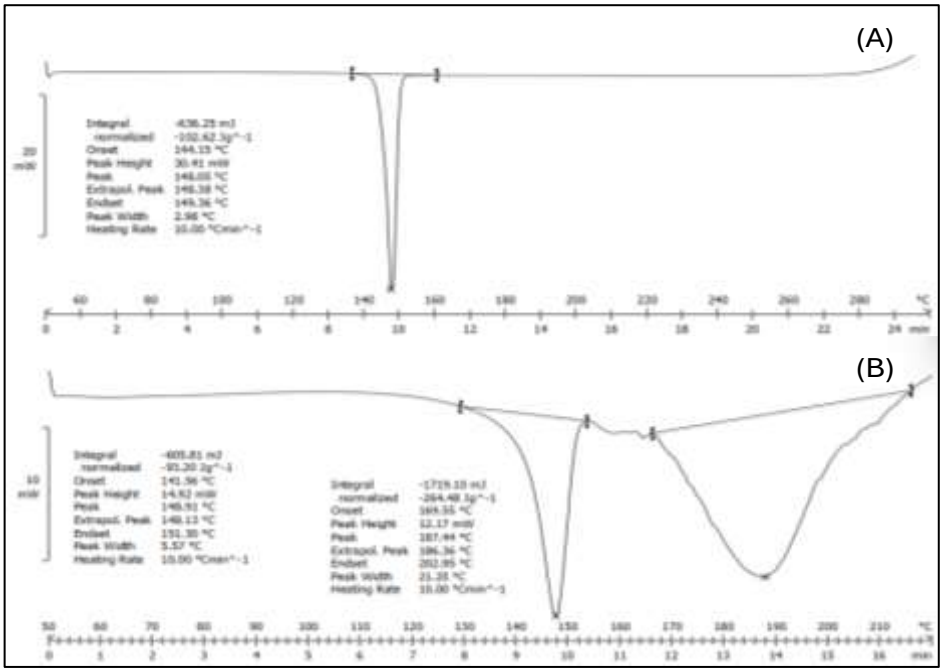


**Figure 2: DSC Spectra of (A) Pure Lappaol F [148.05] and (B) Physical Mixture [148.91 and 187.44]**

**FTIR Analysis**

The FTIR spectra of pure Lappaol F and its physical mixture with formulation excipients are illustrated in Figure 3. The spectrum of pure Lappaol F (Figure 3A) displayed characteristic absorption bands at 3434 $cm^{-1}$ (O–H stretching), 3031–3070 $cm^{-1}$ (aromatic C–H stretching), 2922–2958 $cm^{-1}$ (aliphatic C–H stretching), 1597 $cm^{-1}$ (aromatic C=C stretching), and 1024–1147 $cm^{-1}$ (C–O–C ether stretching), consistent with the lignan structural framework of Lappaol F. The physical mixture spectrum (Figure 3B) retained all principal characteristic peaks of the drug alongside additional excipient bands at 1743 $cm^{-1}$ (C=O ester), 1660 $cm^{-1}$ (amide), and 1173 $cm^{-1}$ (C–O stretching), with no significant peak shifts or disappearance of drug-specific bands, confirming physicochemical compatibility between Lappaol F and all formulation excipients as presented in Table 5. The FTIR spectrum of Lf-LpF-SLNs (Figure 4) revealed characteristic new absorption bands at 1653 $cm^{-1}$ (Amide I) and 1545 $cm^{-1}$ (Amide II), absent in LpF-SLNs, confirming successful covalent lactoferrin surface conjugation. All characteristic Lappaol F and lipid matrix peaks were retained, confirming nanocarrier structural integrity.

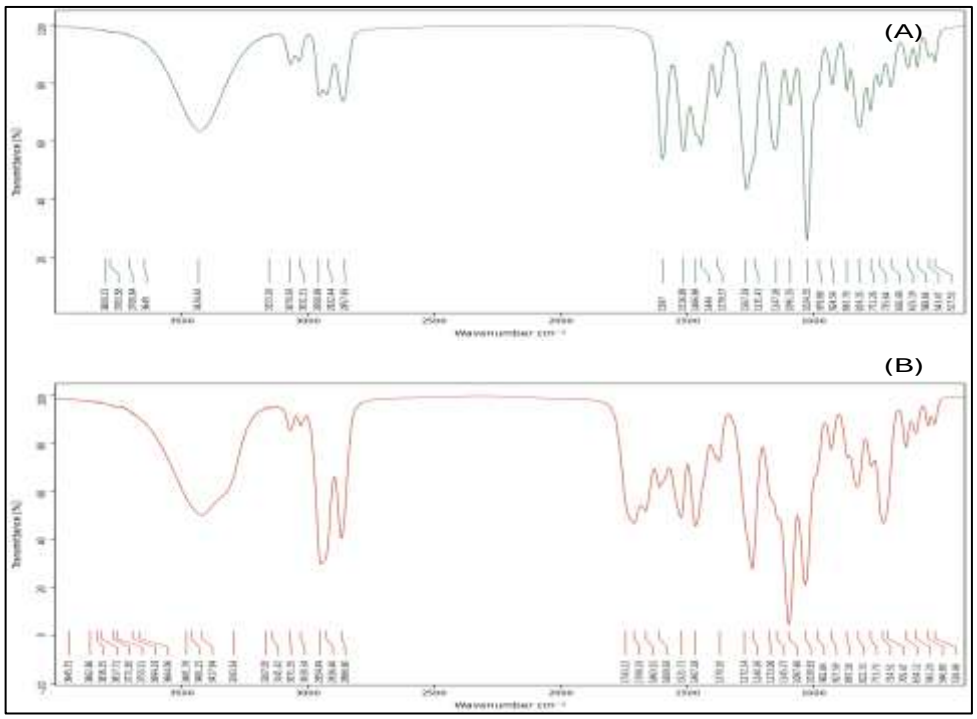


**Figure 3: FTIR Spectra of (A) Pure Lappaol F (B) Physical Mixture (Drug + Excipients) Characterization of Lappaol F-Loaded Solid Lipid Nanocarriers**

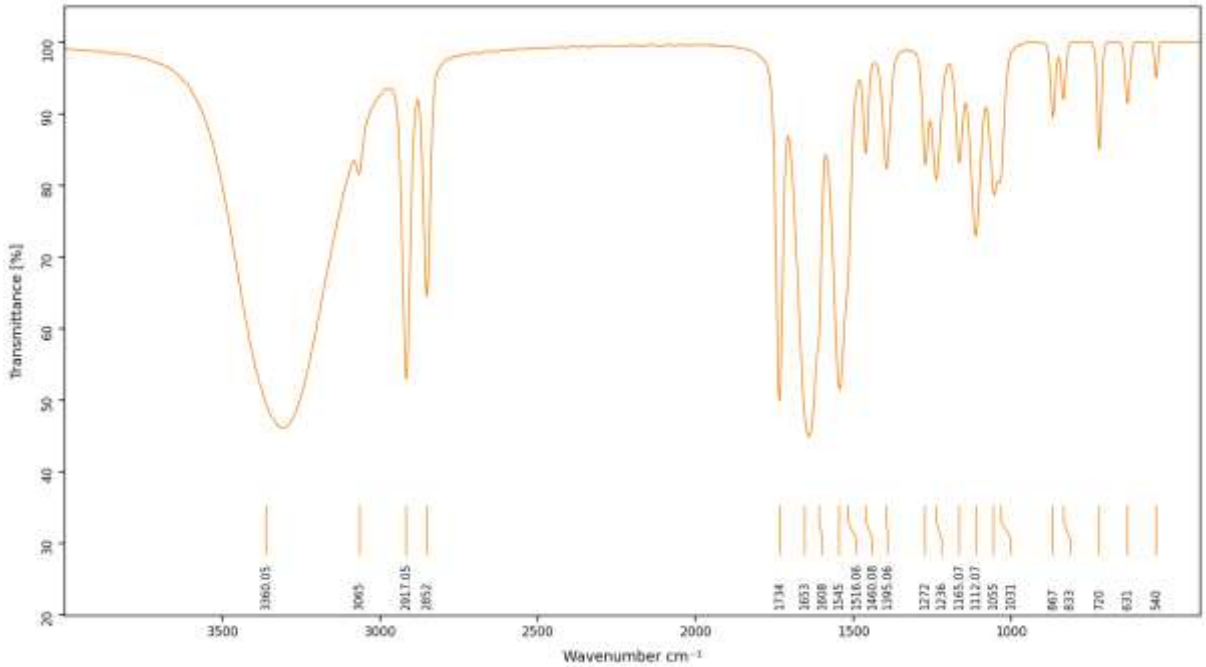


**Figure 4: FTIR Spectra of Lactoferrin Functionalization of Optimized LpF-SLNs**

**Physicochemical Characterization of LpF-SLNs**

The physicochemical parameters of all seventeen Box-Behnken design batches (JF1–JF17) are summarized in Table 5. Particle size ranged from 168.4 ± 4.08 nm (JF12) to 284.6 ± 8.42 nm (JF17), with PDI values between 0.172 ± 0.013 and 0.346 ± 0.034, indicating acceptable size uniformity across most batches. Zeta potential ranged from −14.8 ± 1.62 mV (JF17) to −32.8 ± 1.44 mV (JF12), reflecting adequate colloidal stability. Entrapment efficiency ranged from 54.38 ± 2.64% (JF17) to 81.46 ± 1.68% (JF10), drug content from 88.42 ± 1.58% to 99.18 ± 0.68%, and pH values from 6.46 ± 0.07 to 6.84 ± 0.04, all within acceptable ranges confirming formulation reproducibility.

**Table 5: Physicochemical Characterization of Lappaol F-Loaded Solid Lipid Nanocarriers (JF1–JF17)**

| Batch | Particle Size (nm) | PDI | Zeta Potential (mV) | % EE | Drug Content (%) | % DL | pH |
|---|---|---|---|---|---|---|---|
| JF1 | 189.4 ± 4.12 | 0.212 ± 0.018 | −26.8 ± 1.24 | 74.82 ± 1.84 | 97.84 ± 0.76 | 7.16 ± 0.18 | 6.78 ± 0.04 |
| JF2 | 191.2 ± 3.86 | 0.218 ± 0.021 | −27.1 ± 1.18 | 75.14 ± 1.92 | 98.12 ± 0.82 | 7.19 ± 0.16 | 6.80 ± 0.04 |
| JF3 | 238.6 ± 6.74 | 0.298 ± 0.026 | −19.4 ± 1.42 | 68.46 ± 2.14 | 94.26 ± 1.14 | 5.53 ± 0.22 | 6.64 ± 0.05 |
| JF4 | 178.2 ± 4.58 | 0.186 ± 0.014 | −31.6 ± 1.36 | 79.28 ± 1.76 | 98.64 ± 0.72 | 6.34 ± 0.18 | 6.82 ± 0.04 |
| JF5 | 190.8 ± 3.94 | 0.214 ± 0.019 | −26.4 ± 1.31 | 74.56 ± 1.88 | 97.92 ± 0.78 | 7.14 ± 0.17 | 6.79 ± 0.04 |
| JF6 | 196.4 ± 5.22 | 0.228 ± 0.022 | −24.8 ± 1.28 | 66.34 ± 2.08 | 93.48 ± 1.22 | 7.94 ± 0.21 | 6.62 ± 0.05 |
| JF7 | 262.4 ± 7.86 | 0.318 ± 0.031 | −17.6 ± 1.54 | 61.18 ± 2.36 | 91.36 ± 1.34 | 5.93 ± 0.24 | 6.54 ± 0.06 |
| JF8 | 218.6 ± 5.94 | 0.264 ± 0.024 | −20.2 ± 1.46 | 64.72 ± 2.22 | 93.82 ± 1.18 | 6.26 ± 0.22 | 6.64 ± 0.05 |
| JF9 | 228.8 ± 6.18 | 0.276 ± 0.028 | −22.4 ± 1.38 | 58.84 ± 2.48 | 90.64 ± 1.42 | 7.10 ± 0.26 | 6.52 ± 0.06 |
| JF10 | 172.6 ± 4.34 | 0.178 ± 0.016 | −30.4 ± 1.22 | 81.46 ± 1.68 | 99.18 ± 0.68 | 6.51 ± 0.16 | 6.84 ± 0.04 |
| JF11 | 182.4 ± 4.64 | 0.194 ± 0.017 | −28.6 ± 1.26 | 76.38 ± 1.82 | 98.24 ± 0.74 | 7.30 ± 0.17 | 6.80 ± 0.04 |
| JF12 | 168.4 ± 4.08 | 0.172 ± 0.013 | −32.8 ± 1.44 | 80.62 ± 1.72 | 98.86 ± 0.70 | 7.67 ± 0.16 | 6.83 ± 0.04 |
| JF13 | 214.2 ± 5.68 | 0.246 ± 0.023 | −24.6 ± 1.34 | 72.14 ± 2.06 | 96.42 ± 0.92 | 5.81 ± 0.20 | 6.74 ± 0.05 |
| JF14 | 188.6 ± 3.78 | 0.208 ± 0.016 | −27.4 ± 1.22 | 74.96 ± 1.86 | 97.76 ± 0.78 | 7.17 ± 0.17 | 6.78 ± 0.04 |
| JF15 | 174.8 ± 4.22 | 0.182 ± 0.015 | −30.8 ± 1.32 | 77.84 ± 1.78 | 98.34 ± 0.72 | 7.43 ± 0.17 | 6.81 ± 0.04 |
| JF16 | 198.6 ± 5.14 | 0.234 ± 0.022 | −27.2 ± 1.28 | 71.26 ± 2.12 | 96.88 ± 0.86 | 6.84 ± 0.19 | 6.76 ± 0.05 |
| JF17 | 284.6 ± 8.42 | 0.346 ± 0.034 | −14.8 ± 1.62 | 54.38 ± 2.64 | 88.42 ± 1.58 | 6.60 ± 0.28 | 6.46 ± 0.07 |

All values expressed as mean ± SD (n = 3). PDI: polydispersity index; %EE: percentage entrapment efficiency.

**Optimization of Lappaol F-Loaded Solid Lipid Nanocarriers**

The fit summary for both responses is shown in Table 6. The quadratic model was chosen based on the maximum adjusted $R^2$ values and non-aliased structure as an optimal fit to describe particle size ($Y_1$) and entrapment efficiency ($Y_2$). Sequencing the models confirmed that both responses were best explained by a quadratic model rather than linear and 2FI functional relationships.

**Particle Size ($Y_1$)**

The particle size quadratic model was significantly different (F-value = 8.62, p = 0.0048) with adjusted $R^2$ of 0.8109 showing that the model explained up to 81.09% variability (Table 7). Model adequacy was confirmed by non-significant lack of fit (p = 0.4663). Most notably, significant effects were achieved when Poloxamer 188 (B) was used (F-value = 40.56, p = 0.0004), and Compritol 888 ATO (A) (F-value = 12.20, p = 0.0101). Importantly, the quadratic term $B^2$ (F-value = 15.36, p = 0.0058) was significant suggesting a non-linear relationship between Poloxamer 188 concentration and particle size. Probe sonication pulse duty cycle (C) and all interaction terms were not significant (p > 0.05).

$Y_1 = +192.08 - 17.57A - 32.05B - 11.03C + 8.90AB + 9.15AC + 6.90BC + 3.24A^2 + 27.18B^2 - 3.76C^2$

The negative coefficients of A (−17.57), B (−32.05), and C (−11.03) indicated that increasing all three factors decreased particle size, with the dominating effect being associated with B. At extreme Poloxamer 188 concentrations above the optimum, the coefficient of $B^2$ (+27.18) also denoted an increase in particle size. Response surface and contour plots (Figures 5 and 6) further confirmed minimum particle size at higher combined levels of Compritol 888 ATO and Poloxamer 188 with elevated pulse duty cycle, revealing a steep size reduction gradient that was richest along the Poloxamer 188 axis.

**Entrapment Efficiency ($Y_2$)**

The %EE quadratic model fitted with a high significance (F-value = 10.13, p = 0.0030) and had an adjusted $R^2$ of 0.8370, indicating that the model fit to 83.70% of the response variability (Table 7). There was no significant lack of fit (p = 0.0927). The most important factor having an F-value of 37.74 (p = 0.0005) was Compritol 888 ATO (A), and the second one was Poloxamer 188 (B) with an F-value of 34.85 (p = 0.0006). The large $B^2$ term (F-value = 8.53, p = 0.0223), confirmed non-linear response of %EE to Poloxamer 188 concentration. Interaction terms and factor C remained non-significant (p > 0.05).

$Y_2 = +74.90 + 6.91A + 6.64B + 2.12C - 2.44AB - 1.67AC + 0.3950BC - 1.10A^2 - 4.53B^2 - 1.98C^2$

Positive coefficients of A (+6.91) and B (+6.64) validated the positive contributions of both on %EE, demonstrating a slightly dominant role of Compritol 888 ATO. The significant negative value of $B^2$ coefficient (−4.53) reflected %EE decrement at higher Poloxamer 188 concentrations than the optimal one. The %EE plots (Figures 5 and 6) showed that higher Compritol 888 ATO (4.5–5.0% w/v), together with moderate-to-high Poloxamer 188 (1.0–1.5% w/v), resulted in the maximum %EE (>80%), while the elliptical form of all contour plots suggested that independent variables interact additively, with little to no interaction seen between both factors on entrapment efficiency.

**Table 6: Fit Summary for Particle Size ($Y_1$) and Entrapment Efficiency ($Y_2$)**

| Source | Sequential p-value | Lack of Fit p-value | Adjusted $R^2$ | Predicted $R^2$ | Remark |
|---|---|---|---|---|---|
| **Response 1: Particle Size ($Y_1$)** | | | | | |
| Linear | 0.0016 | 0.1844 | 0.6064 | 0.4197 | Suggested |
| 2FI | 0.6266 | 0.1392 | 0.5669 | −0.0201 | |
| Quadratic | 0.0321 | 0.4663 | 0.8109 | 0.3481 | Suggested |
| Cubic | 0.4663 | — | 0.8139 | — | Aliased |
| **Response 2: Entrapment Efficiency ($Y_2$)** | | | | | |
| Linear | 0.0002 | 0.0566 | 0.7242 | 0.6092 | Suggested |
| 2FI | 0.6107 | 0.0410 | 0.6987 | 0.3576 | |
| Quadratic | 0.0653 | 0.0927 | 0.8370 | 0.0977 | Suggested |
| Cubic | 0.0927 | — | 0.9338 | — | Aliased |

Quadratic model selected as the best-fit model for both responses based on highest Adjusted $R^2$ and non-aliased structure. 2FI: two-factor interaction

**Table 7: ANOVA Summary for Quadratic Model — Particle Size ($Y_1$) and Entrapment Efficiency ($Y_2$)**

| Source | Sum of Squares | df | Mean Square | F-value | p-value | Significance |
|---|---|---|---|---|---|---|
| **Response 1: Particle Size ($Y_1$)** | | | | | | |
| Model | 15725.07 | 9 | 1747.23 | 8.62 | 0.0048 | Significant |
| A: Compritol 888 ATO | 2471.05 | 1 | 2471.05 | 12.20 | 0.0101 | Significant |
| B: Poloxamer 188 | 8217.62 | 1 | 8217.62 | 40.56 | 0.0004 | Significant |
| C: Probe sonication pulse duty cycle | 972.40 | 1 | 972.40 | 4.80 | 0.0646 | — |
| AB | 316.84 | 1 | 316.84 | 1.56 | 0.2513 | — |
| AC | 334.89 | 1 | 334.89 | 1.65 | 0.2394 | — |
| BC | 190.44 | 1 | 190.44 | 0.9400 | 0.3646 | — |
| $A^2$ | 44.06 | 1 | 44.06 | 0.2175 | 0.6551 | — |
| $B^2$ | 3111.68 | 1 | 3111.68 | 15.36 | 0.0058 | Significant |
| $C^2$ | 59.69 | 1 | 59.69 | 0.2946 | 0.6041 | — |
| Residual | 1418.12 | 7 | 202.59 | — | — | — |
| Lack of Fit | 620.63 | 3 | 206.88 | 1.04 | 0.4663 | Not Significant |
| **Response 2: Entrapment Efficiency ($Y_2$)** | | | | | | |

| | | | | | | |
|---|---|---|---|---|---|---|
| Model | 923.22 | 9 | 102.58 | 10.13 | 0.0030 | Significant |
| A: Compritol 888 ATO | 382.26 | 1 | 382.26 | 37.74 | 0.0005 | Significant |
| B: Poloxamer 188 | 352.98 | 1 | 352.98 | 34.85 | 0.0006 | Significant |
| C: Probe sonication pulse duty cycle | 36.12 | 1 | 36.12 | 3.57 | 0.1009 | — |
| AB | 23.81 | 1 | 23.81 | 2.35 | 0.1691 | — |
| AC | 11.09 | 1 | 11.09 | 1.09 | 0.3302 | — |
| BC | 0.6241 | 1 | 0.6241 | 0.0616 | 0.8111 | — |
| $A^2$ | 5.09 | 1 | 5.09 | 0.5030 | 0.5011 | — |
| $B^2$ | 86.40 | 1 | 86.40 | 8.53 | 0.0223 | Significant |
| $C^2$ | 16.59 | 1 | 16.59 | 1.64 | 0.2414 | — |
| Residual | 70.90 | 7 | 10.13 | — | — | — |
| Lack of Fit | 54.46 | 3 | 18.15 | 4.42 | 0.0927 | Not Significant |

p-value < 0.05 considered statistically significant. Lack of Fit p-value > 0.05 for both responses confirms model adequacy. df: degrees of freedom.

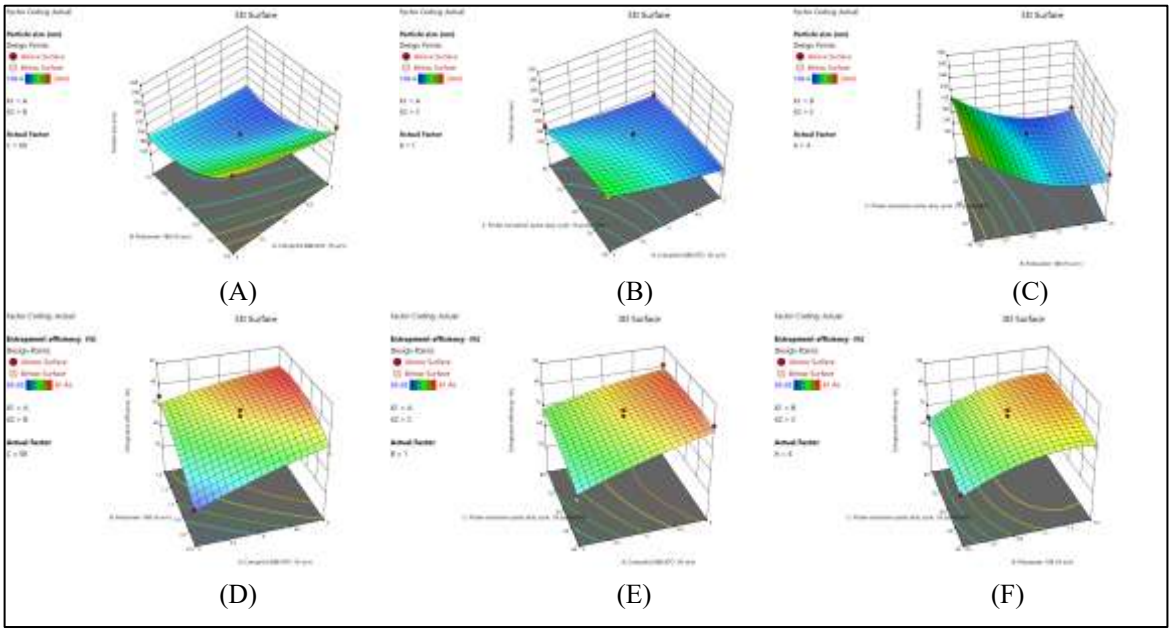


**Figure 5.** Three-dimensional response surface plots illustrating the interactive effects of pairwise combinations of independent variables on the measured responses. Plots (A–C) depict the effect on particle size ($Y_1$): (A) effect of Compritol 888 ATO and Poloxamer 188 on $Y_1$; (B) effect of Compritol 888 ATO and probe sonication pulse duty cycle on $Y_1$; (C) effect of Poloxamer 188 and probe sonication pulse duty cycle on $Y_1$. Plots (D–F) depict the effect on entrapment efficiency ($Y_2$): (D) effect of Compritol 888 ATO and Poloxamer 188 on $Y_2$; (E) effect of Compritol 888 ATO and probe sonication pulse duty cycle on $Y_2$; (F) effect of Poloxamer 188 and probe sonication pulse duty cycle on $Y_2$. In each plot, the third independent variable is held constant at its central (zero) level**.**

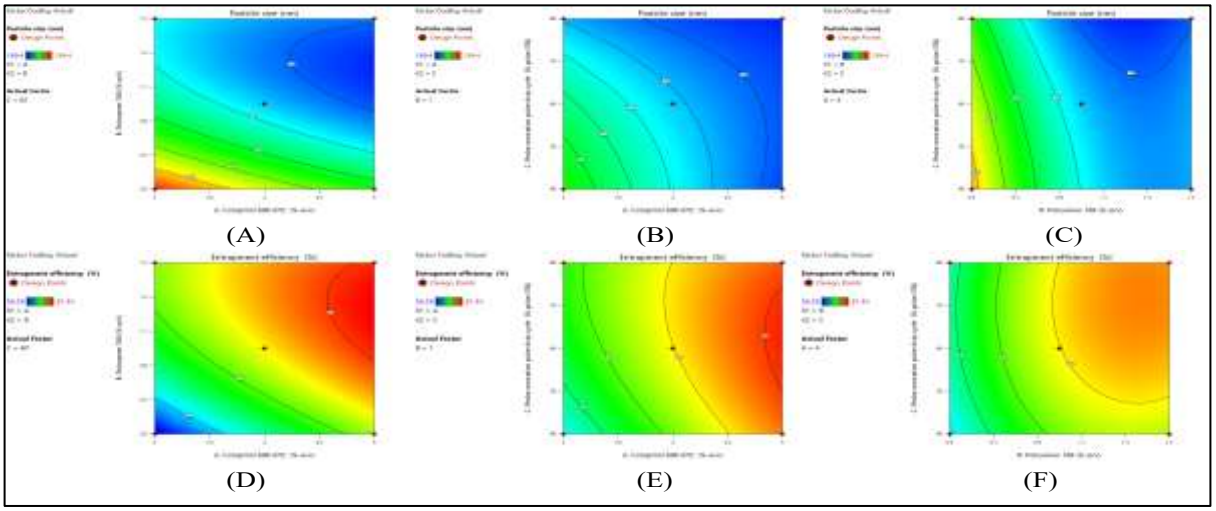


**Figure 6**. Two-dimensional contour plots illustrating the interactive effects of pairwise combinations of independent variables on the measured responses. Plots (A–C) depict the effect on particle size ($Y_1$): (A) effect of Compritol 888 ATO

and Poloxamer 188 on $Y_1$; (B) effect of Compritol 888 ATO and probe sonication pulse duty cycle on $Y_1$; (C) effect of Poloxamer 188 and probe sonication pulse duty cycle on $Y_1$. Plots (D–F) depict the effect on entrapment efficiency ($Y_2$): (D) effect of Compritol 888 ATO and Poloxamer 188 on $Y_2$; (E) effect of Compritol 888 ATO and probe sonication pulse duty cycle on $Y_2$; (F) effect of Poloxamer 188 and probe sonication pulse duty cycle on $Y_2$. In each plot, the third independent variable is maintained at its central (zero) level.

Validation of Statistical model

Among them, the numerical desirability function finally selected the optimal formulation JF10 with an overall desirability of 0.924 (Table 8). The experimental values for particle size (172.6 ± 4.34 nm) and entrapment efficiency (81.46 ± 1.68%) matched closely with the predicted values of 172.100 nm and 79.188% respectively, bearing low relative errors of 0.291% and 2.869%. It is important to mention that the low discrepancy between predicted vs experimental values ensured a high degree of predictive accuracy and robust nature of the developed Box-Behnken quadratic model for optimizing Lappaol F-loaded solid lipid nanocarrier.

**Table 8: Validation of Optimized Formulation (JF10)**

| Batch | Response | Predicted Value | Experimental Value | % Relative Error | Desirability |
|---|---|---|---|---|---|
| **JF10** | Particle Size | 172.100 | 172.6 | 0.291 | 0.976 |
| | Entrapment Efficiency | 79.188 | 81.46 | 2.869 | |

**In Vitro Drug Release studies**

Cumulative drug release profiles of all LpF-SLN formulations (JF1–JF17) within 12 hours were shown in Figure 7 and Table 3. The release at 12 hours was between 61.4 ± 1.56% (JF12) and 87.2 ± 1.96% (JF17), displaying a characteristic biphasic profile with an initial burst release followed by a prolonged sustained-release phase for each batch. The optimized batch JF10 exhibited 63.6 ± 1.58% release at 12 h suggesting controlled sustained release behavior, but JF17 with lowest amount of lipid showed fast release profile.

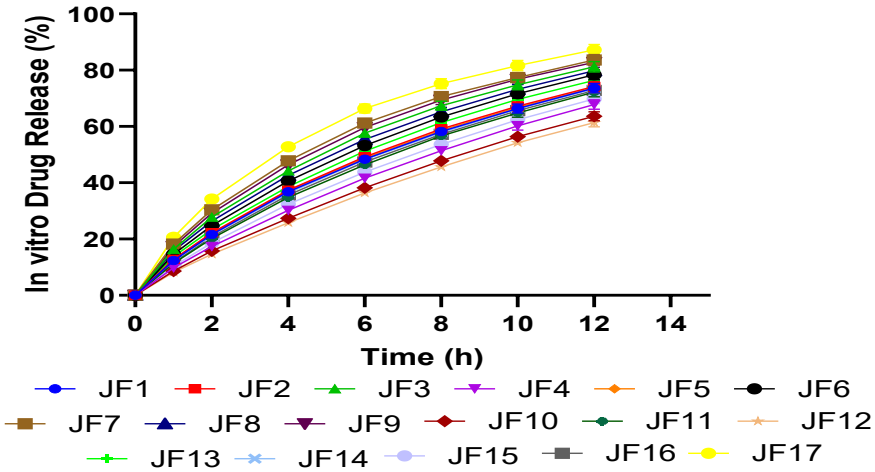


**Figure 7: In Vitro Drug Release profile of all batches F1-F17**

**Results of Release Kinetics**

In vitro drug release of optimized LpF-SLNs (JF10) was fit in five equations, as demonstrated in Figure 8. Out of all the models that were evaluated, highest $R^2 = 0.9999$ was achieved with Hixson-Crowell model which was the best fit, followed by first-order ($R^2 = 0.9988$) and Korsmeyer-Peppas ($R^2 = 0.9991$) models suggesting that both diffusion as well as erosion of lipid matrix occurred during drug release along with simultaneous changes in surface area and diameter of nanoparticles throughout the release process.

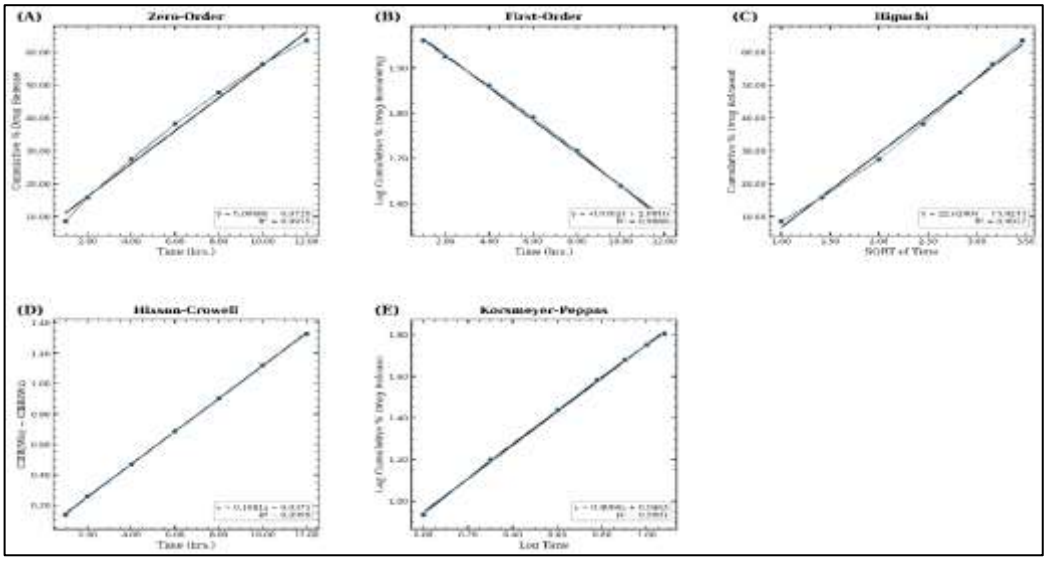


**Figure 8: In vitro drug release kinetics of optimized LpF-SLNs (JF10) fitted to mathematical release models: (A) Zero-order model; (B) First-order model; (C) Higuchi matrix model; (D) Hixson-Crowell model; (E) Korsmeyer-Peppas model.**

**TEM Analysis**

The TEM image of optimized LpF-SLNs (Figure 9) showed uniformly sized, discrete and spherical nanoparticles with smooth surface and evenly distributed particle sizes in the sample. The absence of particle aggregation and coalescence confirmed good colloidal stability. The particle size observed under TEM was comparable with the hydrodynamic diameter of particles as measured by DLS (172.6 ± 4.34 nm), thus confirming successful preparation of nanoscale solid lipid nanocarriers with desirable morphological properties for parenteral administration of cancer drugs.

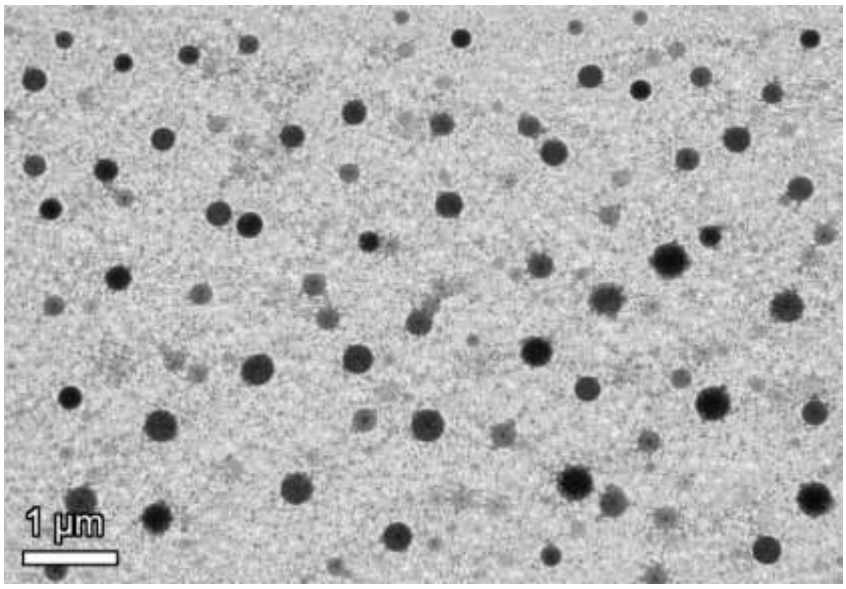


**Figure 9: TEM of Optimized Batch (JF10)**

**Accelerated Stability Studies**

Accelerated stability data of optimized Lf-LpF-SLNs at 40 ± 2°C/75 ± 5% RH over 6 months are presented in Table 9. Particle size marginally increased from 172.6 ± 4.34 nm to 179.6 ± 5.12 nm, PDI from 0.178 ± 0.016 to 0.194 ± 0.021, while zeta potential, %EE, drug content, and pH showed minimal reductions from −30.4 ± 1.22 mV to −27.2 ± 1.42 mV, 81.46 ± 1.68% to 78.18 ± 1.92%, 98.64 ± 0.84% to 95.72 ± 1.02%, and 6.82 ± 0.04 to 6.70 ± 0.06, respectively, with no statistically significant changes ($p > 0.05$), confirming adequate physicochemical stability of Lf-LpF-SLNs throughout the six-month study period as per ICH Q1A(R2) guidelines.

**Table 9: Accelerated Stability Studies of Optimized Lactoferrin-Functionalized Lappaol F-Loaded Solid Lipid Nanocarriers**

| Parameter | Initial (0 Month) | 1 Month | 3 Month | 6 Month |
|---|---|---|---|---|
| Particle Size (nm) | 172.6 ± 4.34 | 173.8 ± 4.52 | 175.8 ± 4.76 | 179.6 ± 5.12 |
| PDI | 0.178 ± 0.016 | 0.182 ± 0.017 | 0.186 ± 0.018 | 0.194 ± 0.021 |

| | | | | |
|---|---|---|---|---|
| Zeta Potential (mV) | -30.4 ± 1.22 | -29.8 ± 1.26 | -28.8 ± 1.32 | -27.2 ± 1.42 |
| % EE | 81.46 ± 1.68 | 80.92 ± 1.72 | 79.84 ± 1.78 | 78.18 ± 1.92 |
| % Drug Content | 98.64 ± 0.84 | 98.12 ± 0.86 | 97.14 ± 0.92 | 95.72 ± 1.02 |
| pH | 6.82 ± 0.04 | 6.80 ± 0.04 | 6.76 ± 0.05 | 6.70 ± 0.06 |

All values expressed as mean ± SD (n = 3).

**In Vitro Cytotoxicity assay**

The cytotoxic activity of free Lappaol F, LpF-SLNs and Lf-LpF-SLNs against MCF-7 cells depending on concentration is shown in Table 10 and Figure 10. Viability progressively decreased with increased concentration in all formulations. $IC_{50}$ of Lf-LpF-SLNs was 14.82 ± 0.92 µg/mL which was smaller compared to that of free Lappaol F (28.64 ± 1.24 µg/mL) and LpF-SLNs (21.38 ± 1.06 µg/mL), demonstrating about 1.93-fold and 1.44-fold better cytotoxicity properties as compared to those of free drug and LpF-SLNs, respectively (Figure 11). Lf-LpF-SLNs at 100 µg/mL had a cell viability that decreased to 7.48 ± 2.18%. Results obtained with inverted microscopy (Figure 10), magnified by 40 times, support these findings showing that Lf-LpF-SLNs-treated cells displayed a drastic phenotype including extensive membrane blebbing and most of them had lost confluence while free Lappaol F and treatment with LpF-SLNs exhibited moderate morphological changes.

**Table 10: In Vitro Cytotoxicity (% Cell Viability) of Free Lappaol F, LpF-SLNs, and Lf-LpF-SLNs against MCF-7 Cell Line**

| Concentration (µg/mL) | Free Lappaol F (% Cell Viability) | LpF-SLNs (% Cell Viability) | Lf-LpF-SLNs (% Cell Viability) |
|---|---|---|---|
| 1 | 92.46 ± 1.84 | 89.62 ± 1.76 | 86.34 ± 1.68 |
| 5 | 82.18 ± 1.92 | 76.44 ± 1.82 | 70.28 ± 1.74 |
| 10 | 68.34 ± 2.14 | 60.82 ± 1.94 | 52.46 ± 1.86 |
| 25 | 48.62 ± 2.28 | 40.16 ± 2.12 | 31.84 ± 1.96 |
| 50 | 32.46 ± 2.42 | 24.38 ± 2.24 | 17.62 ± 2.08 |
| 100 | 18.84 ± 2.56 | 12.64 ± 2.36 | 7.48 ± 2.18 |
| $IC_{50}$ (µg/mL) | 28.64 ± 1.24 | 21.38 ± 1.06 | 14.82 ± 0.92 |

All values expressed as mean ± SD (n = 3). $IC_{50}$ values determined by non-linear regression analysis using GraphPad Prism 9.0.

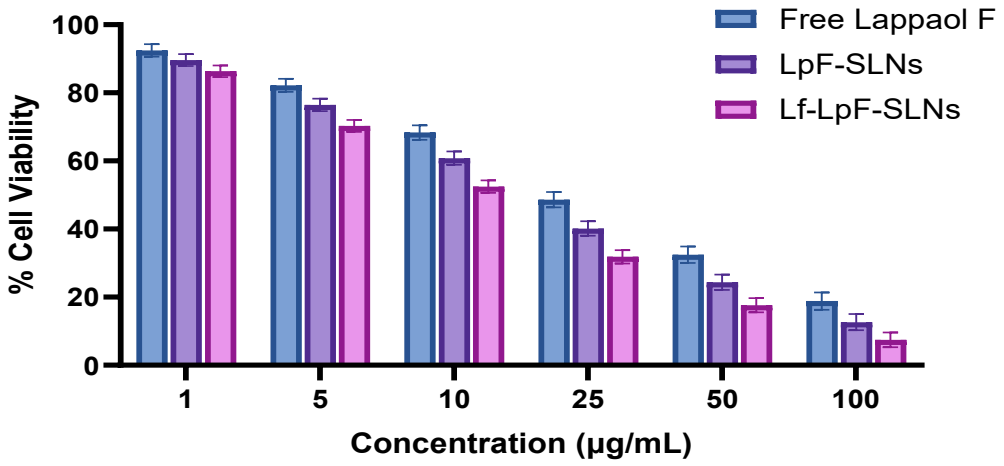


**Figure 10: Concentration-dependent cytotoxic activity of Free Lappaol F, LpF-SLNs, and Lf-LpF-SLNs against MCF-7 human breast adenocarcinoma cell line assessed by MTT assay after 48 hours of treatment at concentrations ranging from 1 to 100 µg/mL. Data expressed as mean ± SD (n = 3).**

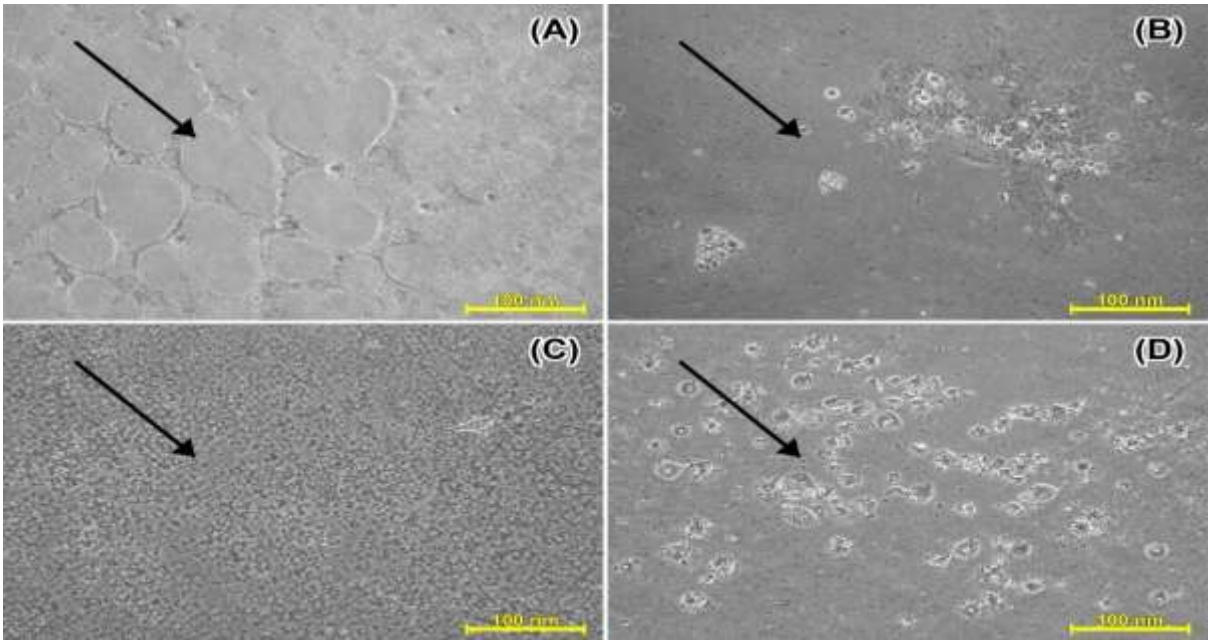


**Figure 11:** Inverted microscopy images of MCF-7 cells after 48 hours of treatment (scale bar = 100 nm): (A) untreated control cells showing intact confluent morphology; (B) Free Lappaol F-treated cells exhibiting moderate cytomorphological changes; (C) Lf-LpF-SLNs-treated cells demonstrating pronounced cell shrinkage, membrane blebbing, and extensive loss of cell confluence indicative of enhanced cytotoxicity; (D) LpF-SLNs-treated cells showing notable but comparatively lesser morphological alterations. Arrows indicate representative regions of cytomorphological changes.

## DISCUSSION

In the current work, using a Quality-by-Design (QbD) tool, we successfully developed and characterized lactoferrin-functionalized Lappaol F-loaded solid lipid nanocarriers (Lf-LpF-SLNs). This preformulation characterization verified that Lappaol F is a highly lipophilic compound (solubility 0.08–0.14 mg/mL in aqueous media, Table 4), which provided strong rationale on its BCS Class IV classification [37] thus strongly warranted encapsulation within a lipid-based nanocarrier system. The crystalline character of Lappaol F and physicochemical compatibilities with all the formulation excipients, assessment of which showed no chemical interactions in the physical mixture were confirmed by DSC and FTIR analyses (Figure 2 and 3), findings that are consistent with preformulation evaluation studies recommended for lignan-class compounds being loaded into lipid nanocarriers [38]. Ultimately, this led to the preliminary trial batches shown in Table 1, which was designed to isolate a set of critical formulation variables within each category of formulation variable: Compritol 888 ATO and Poloxamer 188 as solid matrix and surfactant polymers, respectively, as well as the pulse duty cycle of probe sonication introduced here for the first time as an independent variable into functionalized SLN optimization another novel contribution made by this work that added novelty over similar studies where only amplitude or duration were varied [39]. The Box-Behnken Design optimization resulted in statistically significant quadratic equations for both particle size ($F = 8.62$, $p = 0.0048$, $R^2 = 0.8109$) and entrapment efficiency ($F = 10.13$, $p = 0.0030$, $R^2 = 0.8370$), the respective equations are provided in Tables 6 and 7, with Poloxamer 188 emerging as a factor having dominant control over particle size while Compritol 888 ATO was identified to govern % EE [40,41]. The optimized batch JF10 had particle size 172.6 ± 4.34 nm, PDI of 0.178 ± 0.016, zeta potential -30.4±1.22 mV and %EE (81.46 ± 1.68%) as shown in Table 5; experimentally determined values were found to be in agreement with model predicted values (relative errors being 0.291% and2.869%, Table 8) confirming the robustness of the developed model for predictability of process variables and this confers goodness (Table 7). These physicochemical properties fall well within the ranges reported for anticancer phytochemical-loaded SLN systems targeting solid tumors [42].

Data: The surface functionalization of optimized LpF-SLNs with lactoferrin through EDC/NHS coupling was verified by the FTIR spectroscopy (Figure 4), where specific emergence of Amide I (~1653 $cm^{-1}$) and Amide II (~1545 $cm^{-1}$) absorption bands only in Lf-LpF-SLNs, which were absent from unconjugated LpF-SLNs, gave unambiguous proof for covalent lactoferrin conjugation, described protein-lipid coupling mechanisms similar to those established in transferrin-conjugated SLN-based literature [43]. We focused on lactoferrin, a bifunctional targeting ligand which notably binds to the two overexpressed receptors LRP1 and LRP2, along with lactoferrin-specific receptors in MCF-7 overexpressing breast cancer cells, rendering it as an ideal choice for simultaneous receptor-mediated targeting of lignan-class SLN delivery systems that also enable dual-receptor targeting without requiring separate functionalization mechanisms [44]. Having exhibited characteristic biphasic drug release across all batches in the in vitro release studies (Figure 7, Table 3), the optimized formulation JF10 alone released at a controlled sustained rate of 63.6 ± 1.58% after 12 h, with best data fit through Hixson-Crowell model ($R^2 = 0.9999$) (Figure 8), suggesting simultaneous diffusion and lipid matrix erosion as the governing drug transport mechanism, similar to that reported for Compritol 888 ATO-based SLN systems [45]. The MTT assay revealed a significantly lower $IC_{50}$ of Lf-LpF-SLNs (14.82 ± 0.92 µg/mL) than LpF-SLNs (21.38 ± 1.06 µg/mL) and free Lappaol F (28.64 ± 1.24 µg/mL), indicating a 1.93-fold and 1.44-fold increase in cytotoxicity,

respectively, owing to slactoferrin receptor-mediated active endocytosis resulting in enhanced intracellular delivery of the drug; similar patterns in cytotoxicity activity were found for breast cancer-receptor targeted SLN-frame phytochemical system [46]. Enhanced cytomorphological alterations was further validated by inverted microscopic examination (Figure 11) of the treated cells describing pronounced membrane blebbing and eventual loss of cell confluence in Lf-LpF-SLN treated cells [47]. Accelerated stability studies were performed according to ICH Q1A(R2) guidelines and showed no statistically significant change ($p > 0.05$) of any physicochemical parameter over a six-month period at 40 ± 2°C/75 ±5% RH (Table 9), thus together validating Lf-LpF-SLNs as an active targeted nano-carrier platform with potential for improved bioavailability of drug delivery, and identifying it as a physiochemically stable, cytotoxically superior nanocarrier platform system with substantial preclinical translational potential in the context of breast cancer Lappaol F delivery system [48].

## CONCLUSION

The study successfully developed, optimized, and characterized lactoferrin-functionalized Lappaol F-loaded solid lipid nanocarriers (Lf-LpF-SLNs) by applying a Box-Behnken Design-based QbD approach. The suitability of an optimized formulation JF10 was investigated and found particle size 172.6 ± 4.34 nm, PDI value of 0.178 ± 0.016, zeta potential −30.4 ± 1.22 mV, entrapment efficiency of 81.46 ± 1.68%, whereas sustained release mechanism following the Hixson-Crowell model as governed by $R^2$ value. FTIR spectroscopy substantiated the covalent lactoferrin surface conjugation, and the functionalized nanocarriers revealed significantly higher cytotoxic activity (IC50 of 14.82 ± 0.92 µg/mL) against MCF-7 cells than unconjugated LpF-SLNs or free Lappaol F due to lactoferrin receptor-mediated active targeting. Stability studies under accelerated conditions demonstrated adequate physicochemical stability for six months. These observations establish the clinical translational potential of Lf-LpF-SLNs toward enhanced tumor-selective delivery and improved therapeutic efficacy of Lappaol F, necessitating further in vivo pharmacokinetic, biodistribution, and antineoplastic investigations for the platform progressing towards a clinical use.

## ABBREVIATIONS

ANOVA: Analysis of Variance; BBD: Box-Behnken Design; DLS: Dynamic Light Scattering; DSC: Differential Scanning Calorimetry; EPR: Enhanced Permeability and Retention; FTIR: Fourier-Transform Infrared Spectroscopy; ICH: International Council for Harmonisation; Lf-LpF-SLNs: Lactoferrin-Functionalized Lappaol F-Loaded Solid Lipid Nanocarriers; LpF-SLNs: Lappaol F-Loaded Solid Lipid Nanocarriers; MDR: Multidrug Resistance; MTT: 3-(4,5-Dimethylthiazol-2-yl)-2,5-Diphenyltetrazolium Bromide; PBS: Phosphate-Buffered Saline; PDI: Polydispersity Index; QbD: Quality-by-Design; SD: Standard Deviation; SLN: Solid Lipid Nanocarrier; TEM: Transmission Electron Microscopy; %EE: Percentage Entrapment Efficiency.

**Acknowledgements**

Authors sincerely acknowledge the Principal of institute for providing the necessary laboratory infrastructure, instrumentation facilities and administrative support which led to the successful completion of this research work. The authors would also like to thank Sciquaint Innovations Private Limited, Pune, India for providing Lappaol F and other necessary chemicals free of charge as well as their technical support during the study period. Author contributions LZ, YH and RF designed the study.

## REFERENCES

[1] van Hoogstraten LMC, Vrieling A, van der Heijden AG, Kogevinas M, Richters A, Kiemeney LA. Global trends in the epidemiology of bladder cancer: challenges for public health and clinical practice. Nat Rev Clin Oncol 2023;20:287–304. https://doi.org/10.1038/s41571-023-00744-3.

[2] Santini LA, Temporão JG, Fernandes FMB, Zoss WP, Santos ATC dos. Cancer Control in the 21st Century: Global Challenges Demand Collective Solutions. Rev Bras Cancerol 2025;71:e. https://doi.org/https://doi.org/10.32635/2176-9745.RBC.2025v71n4.5436EN.

[3] Laprise C. It's time to take a sustainable approach to health care in the face of the challenges of the 21st century. One Health 2023;16:100510. https://doi.org/10.1016/j.onehlt.2023.100510.

[4] Rodin G, Feldman A, Trapani D, Skelton M, Unger-Saldaña K, Essue B, et al. The human crisis in cancer: a Lancet Oncology Commission. Lancet Oncol 2025;26:e628–70. https://doi.org/10.1016/S1470-2045(25)00530-3.

[5] Salvo D, Crochemore-Silva I, Wendt A, Tarp J, Shiroma EJ, Simpson RJ, et al. Physical activity for public health in the 21st century. Nat Med 2026:1–11. https://doi.org/10.1038/s41591-026-04237-5.

[6] Meng Q, Li Z, He X, Hu Y, Wu G, Huang J, et al. Anti-TNBC effects of Lappaol F by targeting epithelial-mesenchymal transition via regulation of GSK-3β/YAP/β-catenin and PI3K/AKT pathways. Front Pharmacol 2025;16. https://doi.org/10.3389/fphar.2025.1496511.

[7] Yang R-Y, Tan J-Y, Liu Z, Shen X-L, Hu Y-J. Lappaol F regulates the cell cycle by activating CDKN1C/p57 in human colorectal cancer cells. Pharm Biol 2023;61:337–44. https://doi.org/10.1080/13880209.2023.2172048.

[8] Mankar SD, Tambade AM, Siddheshwar SS, Gawali PS. Development and Fabrication of Zwitterionic Functionalised Mesoporous Silica Nanoparticles of Lappaol F for Breast Cancer. BioNanoScience 2025;15:425. https://doi.org/10.1007/s12668-025-02046-7.

[9] Malaník M, Farková V, Křížová J, Kresová A, Šmejkal K, Kašparovský T, et al. Comparison of Metabolic Profiles of Fruits of Arctium lappa, Arctium minus, and Arctium tomentosum. Plant Foods Hum Nutr 2024;79:497–502. https://doi.org/10.1007/s11130-024-01175-w.

[10] Jacob S, Rao R, Gorain B, Boddu SHS, Nair AB. Solid Lipid Nanoparticles and Nanostructured Lipid Carriers for Anticancer Phytochemical Delivery: Advances, Challenges, and Future Prospects. Pharmaceutics 2025;17:1079. https://doi.org/10.3390/pharmaceutics17081079.
[11] Petrovic SM, Barbinta-Patrascu M-E. Organic and Biogenic Nanocarriers as Bio-Friendly Systems for Bioactive Compounds' Delivery: State-of-the Art and Challenges. Materials 2023;16:7550.
https://doi.org/10.3390/ma16247550.
[12] Zhang J, Mei J, Wang H, Xu Z. Chromatographic fingerprint combined with quantitative analysis of multi-components by single-marker for quality control of total lignans from Fructus arctii by high-performance liquid chromatography. Phytochem Anal 2022;33:1214–24. https://doi.org/10.1002/pca.3172.
[13] Viegas C, Patrício AB, Prata JM, Nadhman A, Chintamaneni PK, Fonte P. Solid Lipid Nanoparticles vs. Nanostructured Lipid Carriers: A Comparative Review. Pharmaceutics 2023;15:1593.
https://doi.org/10.3390/pharmaceutics15061593.
[14] Talarico L, Pepi S, Susino S, Leone G, Bonechi C, Consumi M, et al. Design and Optimization of Solid Lipid Nanoparticles Loaded with Triamcinolone Acetonide. Molecules 2023;28:5747.
https://doi.org/10.3390/molecules28155747.
[15] Cassayre M, Teles de Souza D, Claeys-Bruno M, Altié A, Piccerelle P, Sauzet C. Optimization of Solid Lipid Nanoparticle Formulation Using Design of Experiments, PART I: Strategic Tool for the Determination of Critical Parameters Regarding Formulation and Process. Nanomaterials 2025;15:1034. https://doi.org/10.3390/nano15131034.
[16] Shahab MS, Rizwanullah M, Sarim Imam S. Formulation, optimization and evaluation of vitamin E TPGS emulsified dorzolamide solid lipid nanoparticles. J Drug Deliv Sci Technol 2022;68:103062.
https://doi.org/10.1016/j.jddst.2021.103062.
[17] Li K, Pi C, Wen J, He Y, Yuan J, Shen H, et al. Formulation of the novel structure curcumin derivative–loaded solid lipid nanoparticles: synthesis, optimization, characterization and anti-tumor activity screening in vitro. Drug Deliv 2022;29:2044–57. https://doi.org/10.1080/10717544.2022.2092235.
[18] Correia AC, Moreira JN, Sousa Lobo JM, Silva AC. Design of experiment (DoE) as a quality by design (QbD) tool to optimise formulations of lipid nanoparticles for nose-to-brain drug delivery. Expert Opin Drug Deliv 2023;20:1731–48. https://doi.org/10.1080/17425247.2023.2274902.
[19] Agrawal M, Pradhan M, Singhvi G, Patel R, Ajazuddin, Alexander A. Thermoresponsive *in situ* gel of curcumin loaded solid lipid nanoparticle: Design, optimization and *in vitro* characterization. J Drug Deliv Sci Technol 2022;71:103376. https://doi.org/10.1016/j.jddst.2022.103376.
[20] Khaleseh F, Barzegar-Jalali M, Zakeri-Milani P, Islambulchilar Z, Valizadeh H. Optimum Surfactant Concentration for Preparation of Amiodarone Loaded Solid Lipid Nanoparticles: Theoretical Estimation Versus Experimental Results by Box-Behnken Design. Journal of Reports in Pharmaceutical Sciences; 2024. https://doi.org/10.5812/jrps-146155.
[21] Onugwu AL, Attama AA, Nnamani PO, Onugwu SO, Onuigbo EB, Khutoryanskiy VV. Development and optimization of solid lipid nanoparticles coated with chitosan and poly(2-ethyl-2-oxazoline) for ocular drug delivery of ciprofloxacin. J Drug Deliv Sci Technol 2022;74:103527. https://doi.org/10.1016/j.jddst.2022.103527.
[22] Unnisa A, Chettupalli AK, Al Hagbani T, Khalid M, Jandrajupalli SB, Chandolu S, et al. Development of Dapagliflozin Solid Lipid Nanoparticles as a Novel Carrier for Oral Delivery: Statistical Design, Optimization, In-Vitro and In-Vivo Characterization, and Evaluation. Pharmaceuticals 2022;15:568.
https://doi.org/10.3390/ph15050568.
[23] Satyanarayana SD, Abu Lila AS, Moin A, Moglad EH, Khafagy E-S, Alotaibi HF, et al. Ocular Delivery of Bimatoprost-Loaded Solid Lipid Nanoparticles for Effective Management of Glaucoma. Pharmaceuticals 2023;16:1001. https://doi.org/10.3390/ph16071001.
[24] Khan MFA, Ur. Rehman A, Howari H, Alhodaib A, Ullah F, Mustafa Z ul, et al. Hydrogel Containing Solid Lipid Nanoparticles Loaded with Argan Oil and Simvastatin: Preparation, In Vitro and Ex Vivo Assessment. Gels 2022;8:277. https://doi.org/10.3390/gels8050277.
[25] Yasir M, Zafar A, Noorulla KM, Tura AJ, Sara UVS, Panjwani D, et al. Nose to brain delivery of donepezil through surface modified NLCs: Formulation development, optimization, and brain targeting study. J Drug Deliv Sci Technol 2022;75:103631. https://doi.org/10.1016/j.jddst.2022.103631.
[26] Ho HN, Le HH, Le TG, Duong THA, Ngo VQT, Dang CT, et al. Formulation and characterization of hydroxyethyl cellulose-based gel containing metronidazole-loaded solid lipid nanoparticles for buccal mucosal drug delivery. Int J Biol Macromol 2022;194:1010–8. https://doi.org/10.1016/j.ijbiomac.2021.11.161.
[27] Ramadan AE hakim, Elsayed MMA, Elsayed A, Fouad MA, Mohamed MS, Lee S, et al. Development and optimization of vildagliptin solid lipid nanoparticles loaded ocuserts for controlled ocular delivery: A promising approach towards treating diabetic retinopathy. Int J Pharm X 2024;7:100232.
https://doi.org/10.1016/j.ijpx.2024.100232.
[28] Akbari J, Saeedi M, Ahmadi F, Hashemi SMH, Babaei A, Yaddollahi S, et al. Solid lipid nanoparticles and nanostructured lipid carriers: a review of the methods of manufacture and routes of administration. Pharm Dev Technol 2022;27:525–44. https://doi.org/10.1080/10837450.2022.2084554.
[29] Rao H, Ahmad S, Madni A, Rao I, Ghazwani M, Hani U, et al. Compritol-Based Alprazolam Solid Lipid Nanoparticles for Sustained Release of Alprazolam: Preparation by Hot Melt Encapsulation. Molecules 2022;27:8894. https://doi.org/10.3390/molecules27248894.

[30] Beg S, Malik AK, Ansari MJ, Malik AA, Ali AMA, Theyab A, et al. Systematic Development of Solid Lipid Nanoparticles of Abiraterone Acetate with Improved Oral Bioavailability and Anticancer Activity for Prostate Carcinoma Treatment. ACS Omega 2022;7:16968–79. https://doi.org/10.1021/acsomega.1c07254.
[31] Ramzan M, Gourion-Arsiquaud S, Hussain A, Gulati JS, Zhang Q, Trehan S, et al. In vitro release, ex vivo penetration, and in vivo dermatokinetics of ketoconazole-loaded solid lipid nanoparticles for topical delivery. Drug Deliv Transl Res 2022;12:1659–83. https://doi.org/10.1007/s13346-021-01058-6.
[32] Arabestani MR, Bigham A, Kamarehei F, Dini M, Gorjikhah F, Shariati A, et al. Solid lipid nanoparticles and their application in the treatment of bacterial infectious diseases. Biomed Pharmacother 2024;174:116433. https://doi.org/10.1016/j.biopha.2024.116433.
[33] Noorulla KM, Yasir M, Muzaffar F, S R, Ghoneim MM, Almurshedi AS, et al. Intranasal delivery of chitosan decorated nanostructured lipid carriers of Buspirone for brain targeting: Formulation development, optimization and *In-Vivo* preclinical evaluation. J Drug Deliv Sci Technol 2022;67:102939.
https://doi.org/10.1016/j.jddst.2021.102939.
[34] Parvez S, Karole A, Mudavath SL. Fabrication, physicochemical characterization and *In vitro* anticancer activity of nerolidol encapsulated solid lipid nanoparticles in human colorectal cell line. Colloids Surf B Biointerfaces 2022;215:112520. https://doi.org/10.1016/j.colsurfb.2022.112520.
[35] Emami A, Ghafouri H, Sariri R. Polyphyllin D-loaded solid lipid nanoparticles for breast cancer: Synthesis, characterization, in vitro, and *in vivo* studies. Int J Pharm 2023;639:122976.
https://doi.org/10.1016/j.ijpharm.2023.122976.
[36] Hatami M, Kouchak M, Kheirollah A, Khorsandi L, Rashidi M. Quercetin-loaded solid lipid nanoparticles exhibit antitumor activity and suppress the proliferation of triple-negative MDA-MB 231 breast cancer cells: implications for invasive breast cancer treatment. Mol Biol Rep 2023;50:9417–30. https://doi.org/10.1007/s11033-023-08848-w.
[37] Godase SS, Kulkarni NS, Dhole SN. A comprehensive review on Novel Lipid- Based nano drug delivery. Adv Pharm Bull 2023:1. https://doi.org/10.34172/apb.2024.012.
[38] Fathi F, Machado TOX, de A. C. Kodel H, Portugal I, Ferreira IO, Zielinska A, et al. Solid lipid nanoparticles (SLN) and nanostructured lipid carriers (NLC) for the delivery of bioactives sourced from plants: part II – applications and preclinical advancements. Expert Opin Drug Deliv 2024;21:1491–9. https://doi.org/10.1080/17425247.2024.2410949.
[39] M. SR, S. S. Formulation Design, Optimization, and Evaluation of Solid Lipid Nanoparticles Loaded With an Antiviral Drug Tenofovir Using Box–Behnken Design for Boosting Oral Bioavailability. Adv Pharmacol Pharm Sci 2024;2024:5248746. https://doi.org/10.1155/2024/5248746.
[40] Zarei M, Jonveaux J, Razvi A, Jahn M. Integrated strategy for deep profiling of host cell proteins in downstream processing of therapeutic monoclonal antibodies: Novel approach to isolate and digest host cell proteins. Eur J Pharm Biopharm 2024;201:114369. https://doi.org/10.1016/j.ejpb.2024.114369.
[41] Jacob S, Rao R, Gorain B, Boddu SHS, Nair AB. Solid Lipid Nanoparticles and Nanostructured Lipid Carriers for Anticancer Phytochemical Delivery: Advances, Challenges, and Future Prospects. Pharmaceutics 2025;17:1079. https://doi.org/10.3390/pharmaceutics17081079.
[42] Tran TH, Tran PTT, Truong DH. Lactoferrin and Nanotechnology: The Potential for Cancer Treatment. Pharmaceutics 2023;15:1362. https://doi.org/10.3390/pharmaceutics15051362.
[43] Mostafaei F, Hemmati S, Valizadeh H, Mahmoudian M, Sarfraz M, Abdi M, et al. Enhanced intracellular accumulation and cytotoxicity of bortezomib against liver cancer cells using N-stearyl lactobionamide surface modified solid lipid nanoparticles. Int J Pharm 2024;649:123635. https://doi.org/10.1016/j.ijpharm.2023.123635.
[44] Ozgenc E, Karpuz M, Arzuk E, Gonzalez-Alvarez M, Sanz MB, Gundogdu E, et al. Radiolabeled Trastuzumab Solid Lipid Nanoparticles for Breast Cancer Cell: in Vitro and in Vivo Studies. ACS Omega 2022;7:30015–27. https://doi.org/10.1021/acsomega.2c03023.
[45] Ahmad A, Tabassum H, Nabi R, Mishra A, Ahmad IZ. Solid Lipid Nanoparticles of Lepidium Sativum L Seed Extract: Formulation, Optimization and In vitro Cytotoxicity Studies. Drug Res 2022;72:284–93.
https://doi.org/10.1055/a-1800-5956.
[46] Palei NN, Sabapati M, S V, Samajdar S, Dhar AK. Formulation of Morus alba extract loaded solid lipid nanoparticles: in silico, characterizations, and in vitro cytotoxicity study. Drug Dev Ind Pharm 2025;51:14–28.
https://doi.org/10.1080/03639045.2024.2439930.
[47] Trombino S, Malivindi R, Barbarossa G, Sole R, Curcio F, Cassano R. Solid Lipid Nanoparticles Hydroquinone-Based for the Treatment of Melanoma: Efficacy and Safety Studies. Pharmaceutics 2023;15:1375.
https://doi.org/10.3390/pharmaceutics15051375.
[48] Hanafy MS, Dao HM, Xu H, Koleng JJ, Sakran W, Cui Z. Effect of the amount of cationic lipid used to complex siRNA on the cytotoxicity and proinflammatory activity of siRNA-solid lipid nanoparticles. Int J Pharm X 2023;6:100197. https://doi.org/10.1016/j.ijpx.2023.100197.